

## Hydrodynamic corrections to contact resonance atomic force microscopy measurements of viscoelastic loss tangent

Ryan C. Tung, Jason P. Killgore, and Donna C. Hurley

Citation: *Rev. Sci. Instrum.* **84**, 073703 (2013); doi: 10.1063/1.4812633

View online: <http://dx.doi.org/10.1063/1.4812633>

View Table of Contents: <http://rsi.aip.org/resource/1/RSINAK/v84/i7>

Published by the [AIP Publishing LLC](#).

---

### Additional information on *Rev. Sci. Instrum.*

Journal Homepage: <http://rsi.aip.org>

Journal Information: [http://rsi.aip.org/about/about\\_the\\_journal](http://rsi.aip.org/about/about_the_journal)

Top downloads: [http://rsi.aip.org/features/most\\_downloaded](http://rsi.aip.org/features/most_downloaded)

Information for Authors: <http://rsi.aip.org/authors>

## ADVERTISEMENT

For all your variable temperature, solid state characterization needs....  
... delivering state-of-the-art in technology and proven system solutions  
for over 30 years!

**MMR TECHNOLOGIES**

**Seebeck Measurement Systems**

**Variable Temperature Microprobe Systems**

**Hall Measurement Systems**

**Solutions for Optical Setups!**

Email: [sales@mmr-tech.com](mailto:sales@mmr-tech.com) Web: [www.mmr-tech.com](http://www.mmr-tech.com) Phone: (650) 962-9622 Fax: (888) 522-1011

# Hydrodynamic corrections to contact resonance atomic force microscopy measurements of viscoelastic loss tangent<sup>a)</sup>

Ryan C. Tung,<sup>b)</sup> Jason P. Killgore, and Donna C. Hurley  
*National Institute of Standards and Technology, Boulder, Colorado 80305, USA*

(Received 2 April 2013; accepted 17 June 2013; published online 9 July 2013)

We present a method to improve accuracy in measurements of nanoscale viscoelastic material properties with contact resonance atomic force microscope methods. Through the use of the two-dimensional hydrodynamic function, we obtain a more precise estimate of the fluid damping experienced by the cantilever-sample system in contact resonance experiments, leading to more accurate values for the tip-sample damping and related material properties. Specifically, we consider the damping and added mass effects generated by both the proximity of the cantilever to the sample surface and the frequency dependence on the hydrodynamic loading of the system. The theoretical correction method is implemented on experimental contact resonance measurements. The measurements are taken on a thin polystyrene film and are used to determine the viscoelastic loss tangent,  $\tan \delta$ , of the material. The magnitude of the corrections become significant on materials with low  $\tan \delta$  ( $<0.1$ ) and are especially important for measurements made with the first flexural mode of vibration. [<http://dx.doi.org/10.1063/1.4812633>]

## I. INTRODUCTION

An increasing number of new and emerging applications require information about material properties on the nanoscale. To satisfy these needs, measurement techniques based on atomic force microscopy (AFM) are being developed. In particular, AFM approaches involving contact resonance (CR) methods have been used for quantitative measurements of nanoscale mechanical properties such as elastic modulus.<sup>1–3</sup> More recently, CR techniques have been extended to enable quantitative measurements of nanoscale viscoelastic properties.<sup>4</sup>

Meanwhile, the inclusion of hydrodynamic effects—those caused by a surrounding liquid or gaseous medium—has significantly improved the accuracy of data analysis for many AFM methods. For instance, cantilever spring constant calibration,<sup>5</sup> higher eigenmode spring constant calibration in liquids,<sup>6</sup> and atomic resolution imaging in liquids<sup>7</sup> have all advanced due to the consideration of hydrodynamics. In light of this, it is important to examine how fluid forcing phenomena impact the fidelity of CR measurements.

Here, we examine how hydrodynamics affect CR measurements that use the flexural modes of cantilever vibration to determine viscoelastic properties. We utilize the hydrodynamic function<sup>5,8–10</sup> to describe the fluid mechanics of the system. We present a correction procedure that is readily implemented and accounts for the hydrodynamic loading present in the system. We show that in certain measurement regimes, the effect of these corrections is significant and should not be ignored. This work represents an advancement in CR techniques to achieve more accurate material property data by better accounting for real-world physics.

## II. THEORY

At their core, CR techniques involve measuring the natural frequency  $f$  and quality factor  $Q$  of the AFM cantilever vibration. By measuring  $f$  and  $Q$  both as the cantilever oscillates freely out of contact above the sample surface and while it oscillates with the tip in contact with the sample surface, the sample's viscoelastic properties can be inferred.<sup>4,11</sup> Suitable physical models must be invoked to interpret the measurements. To date, an Euler-Bernoulli model has been utilized to describe the cantilever motion, while a Kelvin-Voigt material model has been used to represent the tip-sample contact. Typically, a Hertzian contact mechanics model is then used to relate the properties of the tip-sample contact to the mechanical properties of the sample. In general, the out-of-contact natural frequency is used to characterize the elastic properties of the cantilever system, and the out-of-contact measurement of  $Q$  is used to quantify the fluid and intrinsic damping present in the CR system.

Heretofore, meticulous care has not been taken to account for the fluid damping in the CR system. Figure 1 conceptually illustrates the two fluid damping effects considered in this work. Figure 1(a) depicts the effect of surface proximity. Previously,<sup>4,12,13</sup> out-of-contact measurements of  $Q$  and  $f$  were made an indeterminate distance away from the sample surface, and all damping unrelated to the sample was ascribed to these measurements. However, it is well known that the proximity of a nearby surface affects the fluid forcing on oscillating microsystems.<sup>10,14,15</sup> The frequency dependence of the fluid damping is another important effect and is depicted in Fig. 1(b). Frequency-dependent fluid effects are especially significant in CR techniques, because relatively large frequency shifts occur between the free and in-contact conditions due to tip-sample interactions.

In this work, we use the two-dimensional hydrodynamic function<sup>10</sup>  $\Gamma$  to account for surface effects. This formulation

<sup>a)</sup>Contribution of NIST, an agency of the US government; not subject to copyright in the United States.

<sup>b)</sup>Electronic mail: ryan.tung@nist.gov

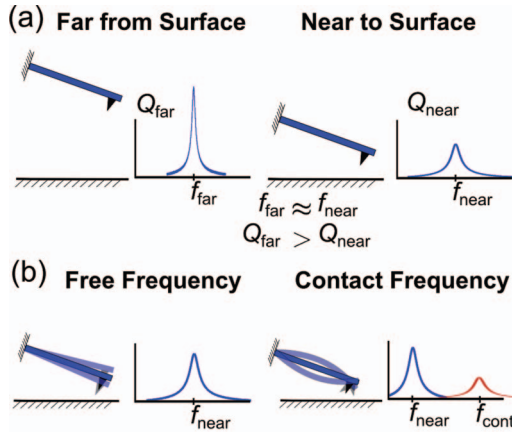


FIG. 1. Fluid damping effects that must be considered in CR spectroscopy.  $f_{\text{far}}$  and  $Q_{\text{far}}$  are the natural frequency and quality factor of the cantilever measured far from the sample surface,  $f_{\text{near}}$  and  $Q_{\text{near}}$  are the natural frequency and quality factor of the cantilever measured near to the sample surface, and  $f_{\text{cont}}$  is the natural frequency of the cantilever when in contact with the sample surface. (a) Surface proximity effects. The quality factor decreases as the cantilever is brought closer to the surface. (b) Frequency dependence of fluid damping. Because  $f_{\text{cont}} > f_{\text{near}}$ , estimations of the fluid damping made at  $f_{\text{near}}$  do not accurately portray the real fluid damping at  $f_{\text{cont}}$ .

arises from the numerical solution of the unsteady Stokes equations,<sup>8</sup> in which it is assumed that the fluid dynamics can be accurately described in a two-dimensional cross-section of the beam-fluid system (that is, there is negligible axial flow along the cantilever's length). Additionally, the model assumes that the cantilever is oriented parallel to the sample surface. Our two-dimensional hydrodynamic assumptions are bolstered both by the small angle of cantilever tilt in the AFM system (typically  $11^\circ$ – $13^\circ$ ) and the increased cantilever-sample gap provided by the long ( $>10 \mu\text{m}$ ) AFM tip, each of which serves to suppress three-dimensional effects.<sup>16,17</sup> We ignore gas compressibility effects and Reynolds-based squeeze film approaches<sup>14,18</sup> due to the relatively low squeeze numbers of the system afforded by the cantilever tilt and increased gap heights. Furthermore, semi-analytical formulas for the calculation of the two-dimensional hydrodynamic function are readily available and easy to use. These formulas have been experimentally validated and computationally verified.<sup>19</sup>

The two-dimensional hydrodynamic function is represented as  $\Gamma(Re, H)$ , where  $Re = (\rho_f \omega b^2)/(4\mu_f)$ ,  $H = 2g/b$ ,  $\rho_f$  is the fluid density,  $\omega = 2\pi f$  is the oscillation frequency,  $b$  is the cantilever beam width,  $\mu_f$  is the fluid viscosity, and  $g$  is the gap height.  $Re$  is the unsteady Reynolds number, the ratio of unsteady inertial forces to viscous forces, while  $H$  is the nondimensional gap height defined by Tung *et al.*<sup>19</sup>  $\Gamma(Re, H)$  is a complex, nondimensional quantity. The real part  $\Gamma_r$  represents the inertial forces of the fluid, or added mass components; whereas the imaginary part  $\Gamma_i$  is proportional to the viscous forces of the fluid, or damping components. The general form of the semi-analytical formula for the hydrodynamic function  $\Gamma$  is  $\Gamma(Re, H) = 10^{\Gamma_L}$  where

$$\Gamma_L(Re_L, H_L) = a_1 + a_2 Re_L + a_3 Re_L^2 + a_4 Re_L^3 + a_5 Re_L^4 + a_6 Re_L H_L + a_7 H_L + a_8 H_L^2 + a_9 H_L^3$$

$$+ a_{10} H_L^4 + a_{11} Re_L H_L^2 + a_{12} Re_L^2 H_L + a_{13} Re_L H_L^3 + a_{14} Re_L^3 H_L + a_{15} (Re_L H_L)^2 + a_{16} (Re_L H_L)^3, \quad (1)$$

$H_L = \log_{10}(H)$ , and  $Re_L = \log_{10}(Re)$ . The coefficients  $a_k$ ,  $k = 1, 2, \dots, 16$ , are complex valued. They are tabulated in Tung *et al.*<sup>19</sup> The fit is valid in the range of  $10^{-2} < Re < 10^4$  and  $10^{-1} < H < 10^1$ .

For a given mode, the vertical deflection response  $w(\omega)$  of the beam system due to harmonic forcing is proportional to<sup>19,20</sup>

$$w(\omega) \propto \frac{1}{1 - M_f \left(\frac{\omega}{\omega_n}\right)^2 + i \tilde{Q}_f^{-1} \left(\frac{\omega}{\omega_n}\right)^2}, \quad (2)$$

where  $\omega_n$  is the  $n$ th natural frequency of the beam. Equation (2) is identifiable as a modified single degree of freedom (SDOF) harmonic oscillator frequency response, where we have neglected the intrinsic damping of the beam. The added mass term  $M_f(Re, H)$  is given by

$$M_f = 1 + \frac{\pi \rho_f b^2}{4m} \Gamma_r(Re, H), \quad (3)$$

where  $m$  is the linear mass density of the beam.  $M_f$  is proportional to the added mass of the surrounding fluid and is governed solely by the real portion of the hydrodynamic function  $\Gamma_r$ . When  $M_f = 1$ , the so-called wet natural frequency<sup>17</sup> (i.e., the natural frequency of the structure immersed in fluid) equals the *in vacuo* natural frequency, and the fluid does not create an added mass effect. The fluid damping of the system is inversely proportional to the variable  $\tilde{Q}_f(Re, H)$  defined by

$$\tilde{Q}_f = \frac{4m}{\pi \rho_f b^2 \Gamma_i(Re, H)}. \quad (4)$$

$\tilde{Q}_f$  is governed solely by the imaginary portion  $\Gamma_i$  of the hydrodynamic function.

In Eqs. (3) and (4), the added mass term  $M_f$  and the damping term  $\tilde{Q}_f$  depend on both frequency and gap height. Herein lies the core of the problem we aim to correct. In reality, the fluid forces experienced by the microcantilever system depend on gap height and frequency, but previous CR work has neglected these effects. To elucidate the phenomena of gap and frequency dependence, Fig. 2(a) shows the quantities  $M_f$  and  $\tilde{Q}_f$  in Eqs. (3) and (4) *versus* gap height  $g$  at the first free natural frequency of the cantilever  $f_1$  and five times the first free natural frequency ( $5f_1$  being near the first contact frequency and slightly below the second free natural frequency). Likewise, Fig. 2(b) shows  $M_f$  and  $\tilde{Q}_f$  *versus* frequency  $f$  at an infinite gap height  $g = \infty$ . The gap height and frequency effects are not independent. We have calculated  $M_f$  and  $\tilde{Q}_f$  at fixed values of  $f$  and  $g$  for illustration purposes. Here, we have input values for the density and viscosity of air at standard temperature and pressure, as well as the nominal properties of the AFM cantilever used in our experiments (see below). For the calculations in Fig. 2(a), we have used Eq. (1) to compute the values of  $\Gamma$ . The calculations in Fig. 2(b) were made with the solution method of Tuck.<sup>9</sup> Figure 2(a) shows that the

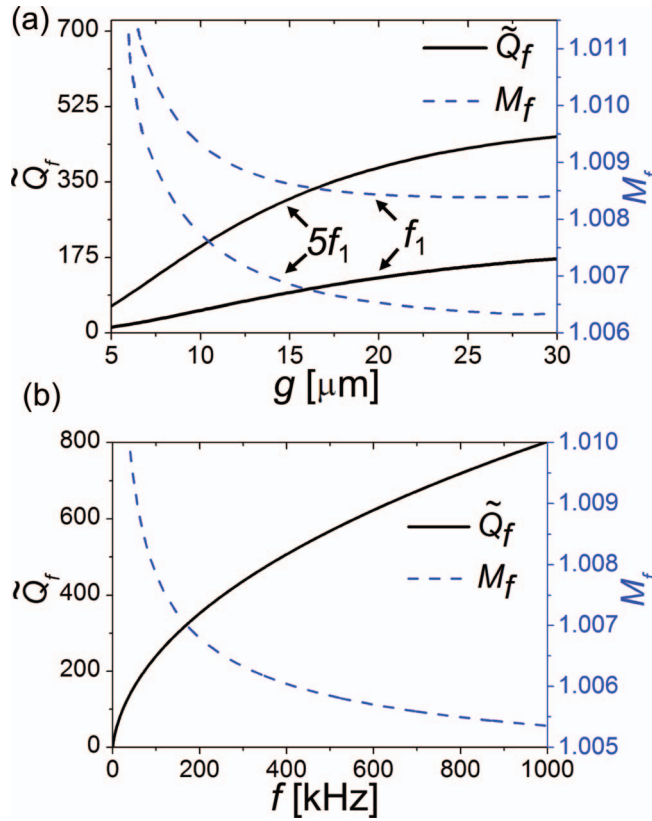


FIG. 2. Added mass and damping effects. (a) Damping term  $\tilde{Q}_f$  and added mass term  $M_f$  vs. gap height  $g$  at the first free natural frequency of the cantilever  $f_1 \approx 75$  kHz and  $5f_1$ . (b) Damping term  $\tilde{Q}_f$  and added mass term  $M_f$  vs. frequency  $f$  at  $g = \infty$ .  $\tilde{Q}_f$  should not be confused with the actual quality factor  $Q$ .  $\tilde{Q}_f$  is inversely proportional to the damping experienced by the system at a particular frequency and gap height and is equal to  $Q$  in special cases.

added mass term in air is quite small, having an overall effect on the *in vacuo* natural frequency of less than 1% across the entire range. As the gap height  $g$  decreases, the damping grows quite large and  $\tilde{Q}_f$  decreases; as  $g$  increases, the damping decreases and  $\tilde{Q}_f$  increases. When  $g$  is larger than several cantilever widths ( $\sim 100 \mu\text{m}$ ), the fluid can be treated as unbounded.<sup>10</sup> In Fig. 2(b), the added mass effect is again minuscule, but the damping term is drastically affected by frequency changes. For example, with our experimental values of  $\sim 75$  kHz for the first free flexural frequency and  $\sim 350$  kHz for the first contact resonance frequency, the increase in  $\tilde{Q}_f$  is more than twofold and therefore should not be overlooked.

Our hydrodynamic correction aims to rectify this situation. Figure 3 depicts a flowchart of the steps involved in the correction. In order to accurately estimate the fluid forces experienced by the in-contact cantilever-sample system, we must first formulate an equivalent cantilever-sample system that is amenable to the two-dimensional hydrodynamic function. This is accomplished by measuring the natural frequency  $f_{\text{near}}$  and quality factor  $Q_{\text{near}}$  of the cantilever very near to the sample surface ( $\sim 250$  nm). With  $f_{\text{near}}$ , we use Eq. (2) to calculate the quality factor as a function of gap height of a fictitious two-dimensional system in which the cantilever is oriented parallel to the sample surface. From these calculations, we determine an equivalent gap height  $g_{\text{equiv}}$  at which

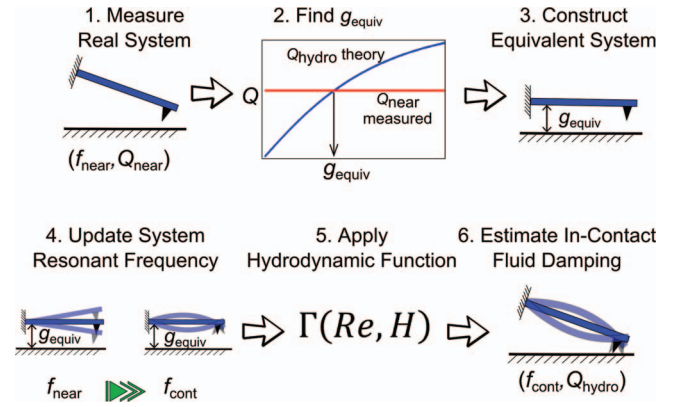


FIG. 3. Flowchart of the hydrodynamic correction procedure.

our two-dimensional system behaves like the measured three-dimensional experimental system. Essentially, we have calibrated our two-dimensional system to match the real experimental system.

Having estimated  $g_{\text{equiv}}$ , we then measure the in-contact resonant frequency  $f_{\text{cont}}$  of the cantilever-sample system. With  $f_{\text{cont}}$  and  $g_{\text{equiv}}$ , we can use Eq. (2) to calculate the in-contact fluid damping  $Q_{\text{hydro}}$ . Applying the approach previously developed for viscoelastic CR analysis<sup>4</sup> and utilizing  $Q_{\text{hydro}}$  and  $f_{\text{hydro}} = f_{\text{cont}}$  for the out-of-contact properties, we then estimate the material properties of the system.

The proposed hydrodynamic correction can be performed on an arbitrary flexural mode of the cantilever. However, it should be noted that with increasing mode number, the assumptions of the two-dimensional hydrodynamic function begin to break down mainly due to increased axial flow (three-dimensional flow). We will show experimentally that the magnitude of the correction decreases with mode number, counteracting this effect.

### III. EXPERIMENTAL METHODS

To test our proposed hydrodynamic correction, we performed CR experiments to determine the viscoelastic loss tangent of a thin supported film of polystyrene (PS).<sup>21</sup> The loss tangent  $\tan \delta$  refers to the phase lag between the applied stress and corresponding strain response, and is equal to the ratio between the viscoelastic loss modulus and storage modulus. A bulk PS sheet<sup>22</sup> was used to prepare the sample. A section of PS sheet was dissolved in toluene at a ratio of 0.125 g polystyrene : 1 ml toluene. Next, the polystyrene-toluene solution was spin-cast onto a silicon wafer to create a film. The sample was then annealed at  $130^\circ\text{C}$  for 12 h. The film thickness of the sample was then measured. A scratch was made on the film, and AFM topography images in intermittent contact mode in the vicinity of the scratch allowed the height between the underlying substrate and the top of the PS film to be measured. The film thickness was determined to be several micrometers, sufficiently thick to prevent substrate effects in the measurement.

A single-crystal silicon cantilever with a thermally measured<sup>23</sup> spring constant of approximately 3.5 N/m was used to conduct the experiments. The nominal length,

width, and thickness of the cantilever were  $225\ \mu\text{m}$ ,  $30\ \mu\text{m}$ , and  $3\ \mu\text{m}$ , respectively. Experiments were conducted with a commercial AFM instrument (MFP-3D, Asylum Research/Oxford Instruments AFM). The cantilever's resonant modes, both in and out of contact, were excited with use of a high-frequency cantilever holder (AM-FM holder, Asylum Research/Oxford Instruments AFM). The acoustic isolation hood was flooded with compressed dry air to maintain a relative humidity of  $<5\%$ , as measured by a hygrometer.

Experiments consisted of the following measurement steps. In each step, 25 measurements were made consecutively for each flexural mode in a  $5 \times 5$  grid corresponding to a region of  $80\ \mu\text{m} \times 80\ \mu\text{m}$ . First, out-of-contact resonance spectra were acquired for the lowest three flexural modes of vibration far from the sample surface ( $>1\ \text{mm}$ ). From the measured frequency response, values of the natural frequency and quality factor far from the sample surface,  $f_{\text{far}}$  and  $Q_{\text{far}}$ , were calculated by a fit to the SDOF harmonic oscillator model. To mitigate nonlinear fluid damping effects, excitation was controlled to keep the peak vibrational amplitudes of the cantilever below  $\sim 1\ \text{nm}$ , as determined from measurements of the photodiode voltage and the cantilever sensitivity.

Next, values for the natural frequency and quality factor near to the sample surface,  $f_{\text{near}}$  and  $Q_{\text{near}}$ , were obtained in a similar fashion. In this case, the cantilever tip was positioned  $250\ \text{nm}$  above the sample surface. This was accomplished by controlling the retraction distance of an amplitude-triggered force-distance measurement.

Finally, values were determined for  $f_{\text{cont}}$  and  $Q_{\text{cont}}$ , the natural frequency and quality factor, respectively, of the cantilever-sample system with the tip in contact. The cantilever was engaged with the sample surface with a force of approximately  $180\ \text{nN}$ . The coupled cantilever-sample system was inertially excited, with the cantilever holder's actuator, and the frequency response was collected and processed as mentioned previously.

#### IV. RESULTS AND DISCUSSION

Results of the measurements described above are given in Table I. The reported values represent the mean and one standard deviation of the 25-measurement sample population. We can see that the contribution of the added mass effect due to the proximity of the sample surface is quite small; that is, the measured values of  $f_{\text{far}}$  and  $f_{\text{near}}$  are identical within measurement uncertainty. Additionally, hydrodynamic calculations show that the contribution of the added mass effect due to frequency dependence is also minimal in this case. From these results, we can conclude that when performed in air, CR

measurements of *frequency alone*, typically used to determine elastic modulus, are virtually unaffected by hydrodynamic effects. It should be noted that this conclusion may not hold in other fluids, such as water, or for extremely short AFM tips.

In contrast, the damping effect due to gap height is quite severe for the first mode, with  $Q_{\text{near}}/Q_{\text{far}} \approx 0.65$ . As the mode number increases, the measured change in damping due to gap height decreases. This can be understood by the fact that higher-order modes have increased unsteady Reynolds numbers, which serve to decrease the contribution of viscous damping. Furthermore, the shorter wavelengths of the higher modes may alleviate gap height effects due to increased axial flow. Also provided in Table I are the measured values of the contact resonance frequency  $f_{\text{cont}}$  and quality factor  $Q_{\text{cont}}$  for the first three flexural modes of coupled vibration. Using the procedure described above, we obtained  $g_{\text{equiv}} = (20.4 \pm 0.3)\ \mu\text{m}$  for the equivalent gap height of the first flexural mode from our measurements and  $g_{\text{equiv}} = (29.5 \pm 0.3)\ \mu\text{m}$  and  $g_{\text{equiv}} = (15.2 \pm 0.1)\ \mu\text{m}$  for the second and third flexural modes, respectively. The nominal tip length of the cantilever used was  $\sim 10\ \mu\text{m}$ . Combined with a nominal cantilever length of  $225\ \mu\text{m}$  and tilt of  $12.5^\circ$ , this yields a value of  $\sim 25\ \mu\text{m}$  for the average cantilever distance from the sample surface when the tip is in contact. This calculation confirms that our estimates for  $g_{\text{equiv}}$  are reasonable. It should be noted that the equivalent gap is a mathematical construct dependent on each mode and *Re* operating regime. As such, the fact that the values are not homogenous across modes is not surprising.

With the results in Table I, we can determine values for the viscoelastic loss tangent  $\tan \delta$  of the polystyrene test sample through the following equation:

$$\tan \delta = \frac{(\lambda L)^2 \beta}{\alpha} \gamma^2 \frac{f_{\text{cont}}}{f_{\text{free}}}. \quad (5)$$

Here,  $\lambda L$  is the root of the dispersion relation for free flexural vibrations of a cantilevered beam<sup>24</sup> for the mode of choice,  $\beta$  is proportional to the damping in the Kelvin-Voigt model,  $\alpha$  is the stiffness of the tip-sample spring in the Kelvin-Voigt model normalized by the cantilever spring constant, and  $\gamma$  is the ratio of tip position to total beam length.  $f_{\text{cont}}$  is the measured contact resonance frequency, and  $f_{\text{free}}$  is the measured free vibration frequency. Equation (5) is a revised version of a formula presented previously<sup>13</sup> and is applicable to arbitrary mode numbers. Methods to determine  $\alpha$ ,  $\beta$ , and  $\gamma$  are described in detail elsewhere.<sup>1,4,12</sup> Using the mode-crossing method,<sup>1</sup> we obtained  $\gamma = 0.9354 \pm 0.0013$  for mode 1 and mode 2 and  $\gamma = 0.9713 \pm 0.0038$  for mode 3.

Table II shows the values of  $\tan \delta$  calculated from the results in Table I, and Figure 4 graphically displays these

TABLE I. Experimental results for the cantilever's natural frequency  $f$  and quality factor  $Q$ .  $f_{\text{far}}$  and  $Q_{\text{far}}$  are measurements taken with the cantilever  $\sim 1\ \text{mm}$  from the sample surface.  $f_{\text{near}}$  and  $Q_{\text{near}}$  are measurements taken with the cantilever tip  $\sim 250\ \text{nm}$  from the sample surface.  $f_{\text{cont}}$  and  $Q_{\text{cont}}$  are measurements taken with the tip in contact with the polystyrene test sample.

Mode #	$f_{\text{far}}$ (kHz)	$f_{\text{near}}$ (kHz)	$f_{\text{cont}}$ (kHz)	$Q_{\text{far}}$	$Q_{\text{near}}$	$Q_{\text{cont}}$
1	$75.13 \pm 0.01$	$75.12 \pm 0.01$	$347.9 \pm 0.7$	$205.2 \pm 1.1$	$132.5 \pm 1.9$	$119.9 \pm 13.6$
2	$476.91 \pm 0.02$	$476.93 \pm 0.02$	$800.7 \pm 10.1$	$585.7 \pm 1.7$	$522.6 \pm 1.3$	$55.3 \pm 21.6$
3	$1340.82 \pm 0.02$	$1340.72 \pm 0.03$	$1454.2 \pm 8.2$	$795.7 \pm 2.6$	$713.9 \pm 2.9$	$163.9 \pm 15.4$

TABLE II. Values of  $\tan \delta$  calculated from the data in Table I with Eq. (5).  $(\tan \delta)_{\text{far}}$  is the viscoelastic loss tangent calculated with the values of  $Q_{\text{far}}$  and  $f_{\text{far}}$  as inputs.  $(\tan \delta)_{\text{near}}$  is calculated with the values of  $Q_{\text{near}}$  and  $f_{\text{near}}$ , while  $(\tan \delta)_{\text{hydro}}$  is calculated with the values of  $Q_{\text{hydro}}$  and  $f_{\text{hydro}}$ .  $\Delta_1$  is the percent difference between  $(\tan \delta)_{\text{far}}$  and  $(\tan \delta)_{\text{near}}$  as defined in the text, and  $\Delta_2$  is the percent difference between  $(\tan \delta)_{\text{far}}$  and  $(\tan \delta)_{\text{hydro}}$ .

Mode #	$(\tan \delta)_{\text{far}}$	$(\tan \delta)_{\text{near}}$	$\Delta_1$ (%)	$f_{\text{hydro}}$ (kHz)	$Q_{\text{hydro}}$	$(\tan \delta)_{\text{hydro}}$	$\Delta_2$ (%)
1	$0.043 \pm 0.005$	$0.039 \pm 0.005$	9.3	$347.9 \pm 0.7$	$374.6 \pm 3.4$	$0.033 \pm 0.005$	23.3
2	$0.028 \pm 0.009$	$0.028 \pm 0.009$	0.0	$800.7 \pm 10.1$	$688.6 \pm 4.5$	$0.027 \pm 0.009$	3.6
3	$0.026 \pm 0.002$	$0.025 \pm 0.002$	3.8	$1454.2 \pm 8.2$	$746.9 \pm 3.8$	$0.025 \pm 0.002$	3.8

results.  $(\tan \delta)_{\text{far}}$  is the value obtained when  $f_{\text{far}}$  and  $Q_{\text{far}}$  are used to characterize the out-of-contact system, while  $(\tan \delta)_{\text{near}}$  is the calculated viscoelastic loss tangent when  $Q_{\text{near}}$  and  $f_{\text{near}}$  are used.  $(\tan \delta)_{\text{hydro}}$  was calculated with the proposed hydrodynamic approach. In Table II,  $\Delta_1 = [(\tan \delta)_{\text{far}} - (\tan \delta)_{\text{near}}]/(\tan \delta)_{\text{far}} \times 100\%$  is the percent difference between the calculated values of  $(\tan \delta)_{\text{far}}$  and  $(\tan \delta)_{\text{near}}$ . Similarly,  $\Delta_2 = [(\tan \delta)_{\text{far}} - (\tan \delta)_{\text{hydro}}]/(\tan \delta)_{\text{far}} \times 100\%$  represents the percent difference between the calculated values of  $(\tan \delta)_{\text{far}}$  and  $(\tan \delta)_{\text{hydro}}$ .

Overall, the values for  $\tan \delta$  are congruous with values in the literature for polystyrene, which range from approximately 0.01 to 0.03 (see, for instance, Refs. 25–27). In addition, we performed dynamic mechanical analysis (DMA) measurements on a specimen from the same PS sheet as used for the CR measurements. Time-temperature superposition analysis of the DMA results estimated  $\tan \delta$  values ranging from 0.02 to 0.04 for oscillation frequencies from 1 Hz to 100 kHz. Although differences in experimental conditions preclude direct comparison of the literature, DMA, and CR results, the values provide useful targets nonetheless. As seen in Fig. 4, our proposed correction has dramatic effects on measurements with the first flexural mode of vibration. As our estimation of the fluid damping becomes more informed, the estimation of the viscoelastic loss tangent decreases by more than 20% and approaches the bulk values. For the second and third modes, the magnitude of the correction decreases to a few percent, but its inclusion remains physically justified.

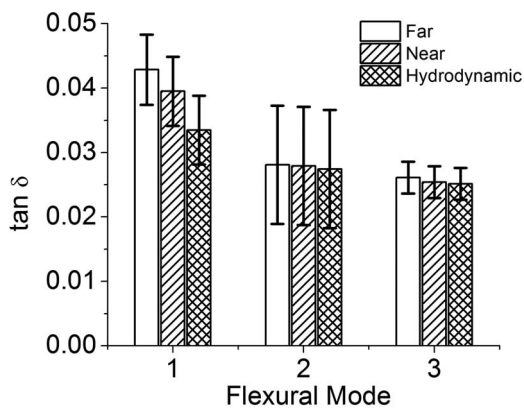


FIG. 4. Contact resonance results for  $\tan \delta$  of polystyrene sample obtained for the first three flexural modes with use of different inputs for the fluid damping estimation. “Far” represents  $\tan \delta$  values calculated with  $Q_{\text{far}}$  and  $f_{\text{far}}$ , “Near” represents  $\tan \delta$  values calculated with  $Q_{\text{near}}$  and  $f_{\text{near}}$ , and “Hydrodynamic” represents  $\tan \delta$  values calculated with  $Q_{\text{hydro}}$  and  $f_{\text{hydro}}$ .

These results suggest the following guidelines for future CR measurements of viscoelastic properties. At a minimum, researchers should measure the fluid damping at a known distance close to the sample surface, as opposed to far from the surface or at an arbitrary distance. Although more calculationally intensive, use of the proposed hydrodynamic correction provides further refinement of the  $\tan \delta$  value. However, room for improvement remains, as the estimation presented here is a two-dimensional hydrodynamic approximation to a three-dimensional system.

At first glance, the values in Tables I and II may appear contradictory, because  $Q_{\text{hydro}}$  is greater than both  $Q_{\text{far}}$  and  $Q_{\text{near}}$ , yet  $(\tan \delta)_{\text{far}}$  is larger than both  $(\tan \delta)_{\text{near}}$  and  $(\tan \delta)_{\text{hydro}}$ . That is, for the same material and  $Q_{\text{cont}}$ , a larger value of  $Q$  used to estimate the fluid damping should result in a larger estimated viscoelastic loss tangent, because more of the damping is being ascribed to the sample surface. However, it is important to remember that for the hydrodynamic correction method we have also updated the relevant frequency values in the calculation and that  $f_{\text{hydro}} = f_{\text{cont}}$  is greater than  $f_{\text{free}}$ . For instance, the parameter  $\bar{\chi} \propto \frac{f_{\text{free}}}{Q_{\text{free}}}$  in Yuya *et al.*<sup>4</sup> would be updated such that  $\bar{\chi} \propto \frac{f_{\text{hydro}}}{Q_{\text{hydro}}}$ .

The corrections discussed here are applicable to the entire measurement regime of CR spectroscopy. In particular, these corrections will significantly improve the accuracy of measurements on materials with low  $\tan \delta$  that employ the first flexural mode of vibration. Hydrodynamic corrections are particularly important for measurements of materials with very low  $\tan \delta$  such as metallic thin films<sup>28</sup> and bulk metallic glasses.<sup>29–31</sup> In such cases, the majority of the measured damping would come from hydrodynamic damping in the system. As the flexural mode number or the value of  $\tan \delta$  increases, the corrections become much less significant, although they are still apropos. With increased mode number comes additional axial flow, along with increased unsteady Reynolds number, both of which reduce the hydrodynamic load. Additionally, at higher modes the ratio between the  $n$ th in-contact vibrational mode and the  $n$ th free vibrational mode decreases, which reduces the frequency-dependent shifts in the hydrodynamic forces.

Figure 5 illustrates this point. To create the plot, we first assumed a constant value for the normalized tip-sample stiffness  $\alpha$ . Using the measured values of  $Q_{\text{near}}$  and the calculated values of  $Q_{\text{hydro}}$  in Table II and  $\gamma = 0.9354$ , we computed  $(\tan \delta)_{\text{near}}$  and  $(\tan \delta)_{\text{hydro}}$  for a range of values of the tip-sample damping term  $\beta$ . In the calculations, we also used theoretically calculated values of the in-contact quality factor  $Q_{\text{cont}}$ , as experimental measurements for a wide

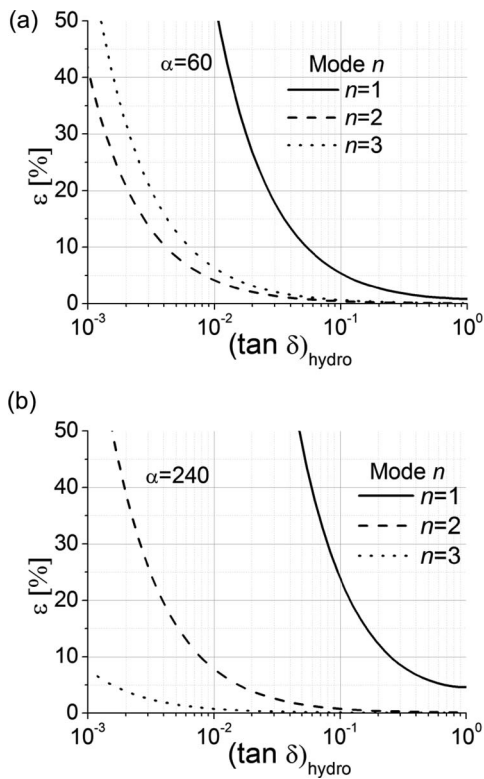


FIG. 5. Here, we have assigned values of  $(\tan \delta)_{\text{hydro}}$  (x-axis) and sample stiffness normalized by cantilever stiffness  $\alpha$ . We use the measured values of  $Q_{\text{near}}$ ,  $\gamma$ , and the calculated values of  $Q_{\text{hydro}}$  for each mode. We assume that  $Q_{\text{hydro}}$  is the actual fluid damping of the system, and compute the percent difference,  $\epsilon$ , between  $(\tan \delta)_{\text{near}}$  calculated with the damping measured close to the surface,  $Q_{\text{near}}$ , and the prescribed theoretical values of  $(\tan \delta)_{\text{hydro}}$ . (a) Results for  $\alpha = 60$ . (b) Results for  $\alpha = 240$ .

range of  $\tan \delta$  were not feasible. The graph in Fig. 5 compares the results of these calculations by graphing the percent difference  $\epsilon = [(\tan \delta)_{\text{hydro}} - (\tan \delta)_{\text{near}}]/(\tan \delta)_{\text{hydro}} \times 100\%$  versus  $(\tan \delta)_{\text{hydro}}$ . It should be noted that this approach assumes  $Q_{\text{hydro}}$  is the actual fluid damping of the system. Figure 5(a) shows calculations for  $\alpha = 60$ , which reflects the experimental conditions. Figure 5(b) was created with  $\alpha = 240$ , which for the same material and cantilever would represent a considerably worn tip or larger applied force. These calculations assume that  $Q_{\text{hydro}}$  is constant while  $\tan \delta$  is varied. In reality,  $Q_{\text{hydro}}$  will vary slightly due to changes in  $f_{\text{cont}}$  as a function of  $\tan \delta$ , but this should not affect the overall trend.

Figure 5 shows that for large values of  $\tan \delta$  ( $\tan \delta \gtrsim 1$ ), the magnitude of the corrections is minimal for both values of  $\alpha$ . However, the percent difference  $\epsilon$  between  $(\tan \delta)_{\text{hydro}}$  and  $(\tan \delta)_{\text{near}}$  increases drastically as  $\tan \delta$  decreases. The first mode is greatly affected, while the second and third mode are relatively unaffected until  $\tan \delta$  is sufficiently decreased ( $\tan \delta \approx 10^{-2}$ ). Figure 5 also suggests that selection of the proper mode(s) for a given measurement is critical to accuracy. The importance of proper mode selection to minimize hydrodynamic damping effects reinforces our previous observations<sup>32</sup> concerning mode selection to maximize measurement sensitivity for a given measurement regime.

## V. CONCLUSIONS

We have presented a method to improve accuracy in measurements of nanoscale viscoelastic material properties with contact resonance AFM methods. Through the use of the two-dimensional hydrodynamic function, we obtained a more realistic estimate of the fluid damping experienced by the cantilever-sample system in CR experiments, leading to more accurate values for the tip-sample damping and related material properties. Specifically, we have considered the effects of damping and added mass generated by the proximity of the cantilever to the sample surface, as well as the frequency dependence of the hydrodynamic loading of the system. The magnitude of the corrections begin become significant on materials with low  $\tan \delta$  ( $<0.1$ ) and are especially important for measurements made with the first flexural mode of vibration. Although they are still valid for higher modes and materials with large  $\tan \delta$ , the magnitude of the correction is much less in these cases. The correction provided by the hydrodynamic function could also have implications in the accurate calculation of energy dissipation and loss tangent from intermittent contact phase imaging<sup>33–35</sup> and the interpretation of quality factor in resonance tracking piezoresponse force microscopy.<sup>36</sup> In general, the effects of the correction will be most pronounced when there are large frequency shifts between free space and feedback-engaged configurations, so corrections for intermittent contact measurements between  $Q_{\text{near}}$  and  $Q_{\text{hydro}}$  will be small compared to contact modes. Overall, the proposed corrections will serve to increase the quantitative accuracy of CR spectroscopy measurements and will bring new light to potential research avenues.

## ACKNOWLEDGMENTS

This research was performed while Ryan C. Tung held a National Research Council Research Associateship Award at the National Institute of Standards and Technology. We thank L. M. Cox and Y. Ding (University of Colorado-Boulder) for DMA measurements and time-temperature superposition analysis.

- <sup>1</sup>U. Rabe, S. Amelio, E. Kester, V. Scherer, S. Hirsekorn, and W. Arnold, *Ultrasonics* **38**, 430 (2000).
- <sup>2</sup>D. C. Hurley, K. Shen, N. M. Jennett, and J. A. Turner, *J. Appl. Phys.* **94**, 2347 (2003).
- <sup>3</sup>M. Kopycinska-Müller, A. Caron, S. Hirsekorn, U. Rabe, H. Natter, R. Hempelmann, R. Birringer, and W. Arnold, *Z. Phys. Chem.* **222**, 471 (2008).
- <sup>4</sup>P. A. Yuya, D. C. Hurley, and J. A. Turner, *J. Appl. Phys.* **109**, 113528 (2011).
- <sup>5</sup>J. E. Sader, *J. Appl. Phys.* **84**, 64 (1998).
- <sup>6</sup>D. Kiracofe and A. Raman, *J. Appl. Phys.* **107**, 033506 (2010).
- <sup>7</sup>T. Fukuma, K. Onishi, N. Kobayashi, A. Matsuki, and H. Asakawa, *Nanotechnology* **23**, 135706 (2012).
- <sup>8</sup>*Laminar Boundary Layers*, edited by L. Rosenhead (Dover Publications, Inc., 1963).
- <sup>9</sup>E. O. Tuck, *J. Eng. Math.* **3**, 29 (1969).
- <sup>10</sup>C. P. Green and J. E. Sader, *J. Appl. Phys.* **98**, 114913 (2005).
- <sup>11</sup>R. Arinero, G. Leveque, P. Girard, and J. Y. Ferrandis, *Rev. Sci. Instrum.* **78**, 023703 (2007).
- <sup>12</sup>J. P. Killgore, D. G. Yablon, A. H. Tsou, A. Gannepalli, P. A. Yuya, J. A. Turner, R. Proksch, and D. C. Hurley, *Langmuir* **27**, 13983 (2011).
- <sup>13</sup>S. E. Campbell, V. L. Ferguson, and D. C. Hurley, *Acta Biomater.* **8**, 4389 (2012).

- <sup>14</sup>T. Vejjola, *J. Micromech. Microeng.* **14**, 1109 (2004).
- <sup>15</sup>M. Bao and H. Yang, *Sens. Actuators, A* **136**, 3 (2007).
- <sup>16</sup>R. J. Clarke, O. E. Jensen, J. Billingham, and P. M. Williams, *Proc. R. Soc. London, Ser. A* **462**, 913 (2006).
- <sup>17</sup>S. Basak, A. Raman, and S. V. Garimella, *J. Appl. Phys.* **99**, 114906 (2006).
- <sup>18</sup>R. C. Tung, J. W. Lee, H. Sumali, and A. Raman, *J. Micromech. Microeng.* **21**, 025003 (2011).
- <sup>19</sup>R. C. Tung, A. Jana, and A. Raman, *J. Appl. Phys.* **104**, 114905 (2008).
- <sup>20</sup>X. Xu and A. Raman, *J. Appl. Phys.* **102**, 034303 (2007).
- <sup>21</sup>Commercial equipment, instruments, or materials are identified only in order to adequately specify certain procedures. In no case does such identification imply recommendation or endorsement by the National Institute of Standards and Technology, nor does it imply that the products identified are necessarily the best available for the purpose.
- <sup>22</sup>Goodfellow USA, Polystyrene Sheet ST313120, see <http://www.goodfellowusa.com>; accessed 3/1/2013.
- <sup>23</sup>H. J. Butt and M. Jaschke, *Nanotechnology* **6**, 1 (1995).
- <sup>24</sup>S. S. Rao, *Vibration of Continuous Systems* (John Wiley and Sons, 2007).
- <sup>25</sup>M. F. Ashby, *Acta Metall.* **37**, 1273 (1989).
- <sup>26</sup>O. Araki, T. Shimamoto, T. Yamamoto, and T. Masuda, *Polymer* **42**, 4433 (2001).
- <sup>27</sup>N. Patra, M. Salerno, A. Diaspro, and A. Athanassiou, *Microelectron. Eng.* **88**, 1849 (2011).
- <sup>28</sup>A. Caron and W. Arnold, *Acta Mater.* **57**, 4353 (2009).
- <sup>29</sup>M. F. Ashby and A. L. Greer, *Scr. Mater.* **54**, 321 (2006).
- <sup>30</sup>C. Haon, D. Camel, B. Drevet, and J. M. Pelletier, *Metall. Mater. Trans. A* **39**, 1791 (2008).
- <sup>31</sup>H. Wagner, D. Bedorf, S. Kuechemann, M. Schwabe, B. Zhang, W. Arnold, and K. Samwer, *Nature Mater.* **10**, 439 (2011).
- <sup>32</sup>J. P. Killgore and D. C. Hurley, *Nanotechnology* **23**, 055702 (2012).
- <sup>33</sup>J. P. Cleveland, B. Anczykowski, A. E. Schmid, and V. B. Elings, *Appl. Phys. Lett.* **72**, 2613 (1998).
- <sup>34</sup>J. Tamayo and R. Garcia, *Appl. Phys. Lett.* **73**, 2926 (1998).
- <sup>35</sup>R. Proksch and D. G. Yablon, *Appl. Phys. Lett.* **100**, 073106 (2012).
- <sup>36</sup>S. Jesse and S. V. Kalinin, *J. Phys. D: Appl. Phys.* **44**, 464006 (2011).